Check for updates

Formation mechanism of multilayer TiO$_2$ nanotubes in HBF$_4$ electrolyte

Shaoyu Zhang,[ab] Mengshi Yu,[a] Liming Xu,[b] Siwei Zhao,[a] Jianfei Che[a] and Xufei Zhu [ID] *[a]

Multilayer anodic TiO$_2$ nanotubes are first fabricated in HBF$_4$-containing electrolyte by a one-step galvanostatic anodization. These nanotubes demonstrate unique A-shaped sidewalls, which are different from the traditional V-shaped nanotubes formed in NH$_4$F-containing electrolyte. Further, the formation mechanism of the multilayer TiO$_2$ nanotubes is proposed. During the anodizing process, the total anodizing current could be separated into ionic current and electronic current. The oxygen bubbles, induced by the electronic current, play a significant role in shaping the nanotube architectures. The bottoms of TiO$_2$ nanotubes could be broadened under the pressure of oxygen bubbles. Thus the wall at the bottom of the nanotube becomes thinner. When the pressure of oxygen bubbles reaches a certain value, it will break the sidewalls of the nanotubes, resulting in the formation of the A-shaped sidewalls of TiO$_2$ nanotubes. However, in NH$_4$F-containing electrolyte, the oxygen bubbles escape from the top of nanotubes, and then the V-shaped sidewall thickness profiles of TiO$_2$ nanotubes are formed. Owing to the inflating effect of oxygen bubbles on the nanotube walls, the whole TiO$_2$ nanotube layer is finally divided into nanotube multilayers in HBF$_4$-containing electrolyte.

Introduction

In recent years, anodic TiO$_2$ nanotubes have received increasing attention due to their various applications.[1–5] The most widely used electrolytes are F$^-$-containing electrolytes.[6–9] Macak *et al.*[7] indicated that the formation of a soluble complex $[TiF_6]^{2-}$ gives rise to oxide dissolution during formation of anodic TiO$_2$ nanotubes. The growth of anodic TiO$_2$ nanotubes is considered to be as a result of the equilibrium between oxide formation and oxide dissolution. The corresponding theory is called field-assisted dissolution mechanism.[7–9]

However, the F$^-$ ion is highly aggressive and restricts the length of TiO$_2$ nanotubes to a few micrometers.[10,11] Furthermore, the field-assisted dissolution mechanism, which is based on the dissolution effect of F$^-$ ions, is doubted because researchers have found that anodic TiO$_2$ nanotubes could be formed in F$^-$-free electrolytes, such as sulfuric acid (H$_2$SO$_4$) electrolyte,[12] silver nitrate (AgNO$_3$) electrolyte[13] and nitric acid (HNO$_3$) electrolyte.[14] In 2015, Hebert *et al.*[15] also indicated that oxide dissolution rates are in fact very small during anodization. In 2012, Yang *et al.*[16–18] elucidated the variation of the anodizing current *versus* time based on an electronic current and oxygen bubble model. They indicated that the total anodizing current

consists of ionic current and electronic current during anodization of Ti.[16–18] Ionic current is used to form oxide while the electronic current gives rise to the evolution of oxygen bubbles. Oxygen bubbles act as moulds during oxide growth.[16–18] Therefore, newly formed oxide flows around these oxygen bubbles and forms anodic TiO$_2$ nanotubes.[16–19] Otherwise, the introduction of new electrolyte is helpful for exploiting new architectures and understanding the formation mechanism of anodic TiO$_2$ nanotubes. Although anodic TiO$_2$ nanotubes have been obtained in HBF$_4$-containing electrolyte, none novel architecture of anodic TiO$_2$ nanotube has been reported. There are few papers reporting forming mechanism of anodic TiO$_2$ nanotubes in HBF$_4$-containing electrolyte.[20]

Anodic TiO$_2$ nanotubes are usually obtained under potentiostatic conditions. Anodizing voltage is generally considered as one of the key influence factors of tube diameter, interpore spacing and barrier layer thickness.[20–23] Galvanostatic anodization is not commonly employed for several reasons including: (a) galvanostatic anodization demands a more accurate control of all experimental factors (area, temperature, hydrodynamics) than potentiostatic anodization,[24] (b) voltage may change with time and fluctuate, and thus it is difficult to control tube diameter,[25] (c) oxide layer is easy to breakdown at high anodizing current. However, Zhang *et al.*[26] indicated that constant current condition is good for quantitative studies of forming mechanism of anodic TiO$_2$ nanotubes. They put forward an equation between nanotube length and anodizing current.[26]

[a]Key Laboratory of Soft Chemistry and Functional Materials of Education Ministry, Nanjing University of Science and Technology, Nanjing 210094, China. E-mail: zhuxufei.njust@163.com

[b]Jiangsu Urban and Rural Construction College, Changzhou 213147, China

Multilayer TiO_2 nanotubes have been prepared in F^--containing electrolyte by several groups. There are bamboo-type nanotubes,[27] Y-branched nanotubes[28] and reverse Y-branched nanotubes.[29,30] These nanotubes have unique performances, such as improvement of dye loading ability for dye-sensitized solar cells.[30] However, multilayer TiO_2 nanotubes formed in HBF_4-containing electrolyte have not been reported. In the present work, we compare anodic TiO_2 nanotubes formed in different electrolytes. Novel multilayer TiO_2 nanotubes were formed in HBF_4-containing electrolyte, while a nanotube single layer was formed in NH_4F-containing electrolyte. Moreover, TiO_2 nanotubes formed in HBF_4-containing electrolyte show an A-shaped sidewall thickness profile, while nanotubes formed in HBF_4-containing electrolyte show a V-shaped thickness profile. The A-shaped sidewall thickness profile is hardly to be explained by tradition field-assisted dissolution mechanism. Thus we proposed a new forming mechanism of the multilayer TiO_2 nanotubes from the perspective of electronic current. The present results may facilitate the development of new electrolytes for preparing anodic TiO_2 nanotubes with various architectures, and also promote the understanding of the forming mechanism.

Experimental details

TiO_2 nanotubes were formed by anodizing of Ti foils. Prior to the anodization, the commercial titanium foils (100 μm thick, purity 99.5%, Shanghai Shangmu Technology Co. Ltd.) were polished in a mixture solution of HF (≥40%), HNO_3 (65–68%) and deionized water (1 : 1 : 2 in volume) for about 10 s, followed by dipping them into deionized water, and dried in the air. The polished Ti foils were then anodized in a two electrodes cell. A current density of 10 mA cm^{-2} was applied between a Ti anode and a Pt cathode. Anodizing experiments were carried out at room temperature (~20 °C) for 15 minutes with stirring of the electrolyte. After anodizations, samples were rinsed with water and dried in air.

The anodization was carried out in ethylene glycol electrolyte with 0.015 M (1.18 wt%) HBF_4 and 2 wt% H_2O (called HBF_4-containing electrolyte). For comparison, anodization of Ti foil in NH_4F-containing electrolyte was studied. NH_4F-Containing electrolyte was ethylene glycol solution containing 0.06 M NH_4F and 2 wt% H_2O. Hence, the concentrations of fluorine in two electrolytes are equal.

The voltage–time curves were recorded automatically by a computer system. Morphologies of both samples were characterized by field-emission SEM (FESEM, Hitachi S-4800 II and Zeiss Supra 55). Nanotube lengths and diameters were all measured directly on the FESEM.

Results and discussion

Multilayer TiO_2 nanotubes formed in HBF_4-containing electrolyte

Fig. 1 shows the multilayer TiO_2 nanotubes formed in HBF_4-containing electrolyte, which are composed of eight TiO_2 nanotube layers (Fig. 1a). Neighboring nanotubes in all layers
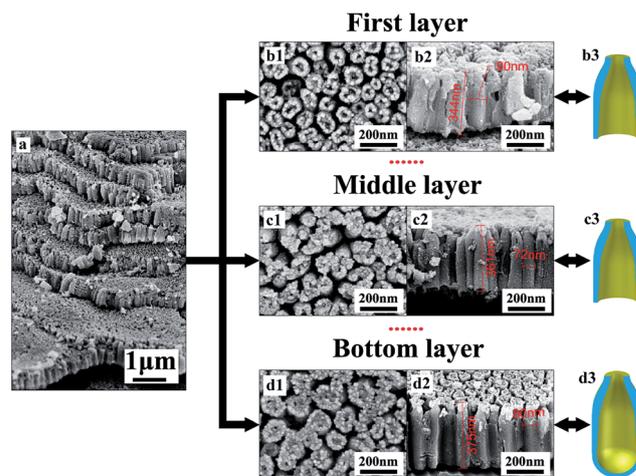

Fig. 1 (a) Cross-sectional FESEM images of multilayer TiO_2 nanotubes formed in HBF_4-containing electrolyte. Top view FESEM images of (b1) the first TiO_2 nanotube layer, (c1) one of middle TiO_2 nanotube layers and (d1) bottom TiO_2 nanotube layer. Cross-sectional FESEM images of (b2) the first TiO_2 nanotube layer, (c2) one of middle TiO_2 nanotube layers and (d2) bottom TiO_2 nanotube layer. Schematic diagram of cross-section of TiO_2 nanotubes in (b3) the first TiO_2 nanotube layer, (c3) one of middle TiO_2 nanotube layers and (d3) bottom TiO_2 nanotube layer.

are separated by gaps (Fig. 1b1–d1). The thickness of each layer is about 360 nm (Fig. 1b2–d2). The outer diameters of nanotubes in the first layer are approximately 90 nm (Fig. 1b2) while outer diameters of nanotubes in middle layer and bottom layer are approximately 72 nm (Fig. 1c2) and 80 nm (Fig. 1d2), respectively. Nanotubes in the first layer and middle layer have through-holes (Fig. 1b2 and c2), while nanotubes in the bottom layer are sealed at bottom by the underlying barrier layer (Fig. d2). In the first layer and middle layer, nanotube walls at the bottom are extremely thin (Fig. 1b2 and c2). Therefore, inner diameters are close to outer diameters at the bottom of nanotubes in the first layer and middle layer. However, inner diameters at the top of nanotubes in the first layer, middle layer and bottom layer are only a few nano meters (Fig. 1b1–d1). Gaps between nanotubes are larger at the top than that at the bottom in first layer, middle layer and bottom layer.

Fig. 2 demonstrates the difference between nanotubes obtained in NH_4F-containing electrolyte and HBF_4-containing electrolyte. Nanotubes formed in HBF_4-containing electrolyte show an A-shaped sidewall thickness profile, while nanotubes formed in NH_4F-containing electrolyte show a V-shaped sidewall thickness profile. In traditional NH_4F-containing electrolyte, ordered TiO_2 nanotubes can be formed and the top nanotube surface is a porous plane. As Kowalski et al.[31] indicated, the dissolution of oxide would form gaps between pores. However, there are no gaps between pores on the top surface (Fig. 2a). Therefore, the oxide dissolution on the surface is negligible. This result is consistent with the previously reported work by Çapraz et al.[15] The cross-sectional SEM images of nanotubes formed in NH_4F-containing electrolyte show perfectly straight and densely packed arrays of TiO_2 nanotubes and the nanotubes are vertically aligned to the Ti substrate.
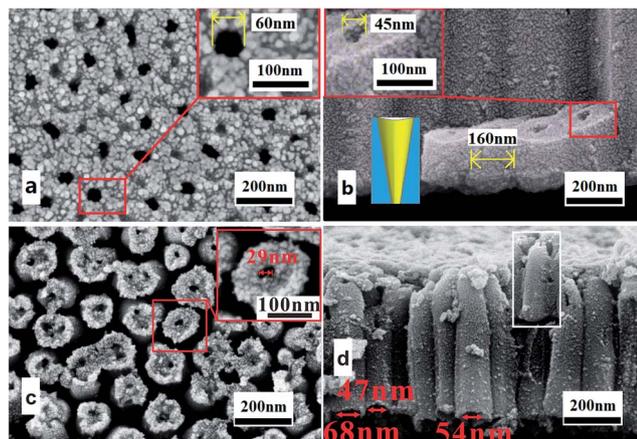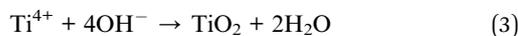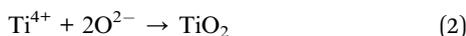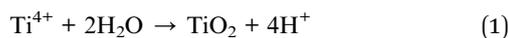
Fig. 2 (a) and (b) FESEM images of the V-shaped TiO_2 nanotubes formed in NH_4F-containing electrolyte. (c) and (d) FESEM images of the A-shaped TiO_2 nanotubes formed in HBF_4-containing electrolyte.

Their outer diameters are approximately 160 nm (Fig. 2b). The inner diameter of the nanotubes is larger on the top (~60 nm, Fig. 2a) than that at the bottom (~45 nm, Fig. 2b). Thus, TiO_2 nanotubes formed in NH_4F-containing electrolyte show a V-shaped structure[26,32] in their thickness (Fig. 2b), in agreement with previous reports.[26,32] For TiO_2 nanotubes formed in HBF_4-containing electrolyte, the inner diameter on the top is much smaller than that at the bottom as shown in Fig. 2c and d. As a result, TiO_2 nanotubes formed in HBF_4-containing electrolyte show an A-shaped structure.

Forming mechanism of multilayer anodic TiO_2 nanotubes

Researchers have presented several growth mechanisms for anodic TiO_2 nanotubes.[25,26,34] Among these mechanisms, the generally accepted mechanism is field-assisted dissolution mechanism. According to field-assisted dissolution mechanism, growth of TiO_2 nanotubes can be ascribed to the dynamic equilibrium between growth (eqn (1)–(3)) and dissolution processes (eqn (4)) of oxide.[21,22,35–38]

$$Ti^{4+} + 2H_2O \rightarrow TiO_2 + 4H^+ \tag{1}$$

$$Ti^{4+} + 2O^{2-} \rightarrow TiO_2 \tag{2}$$

$$Ti^{4+} + 4OH^- \rightarrow TiO_2 + 2H_2O \tag{3}$$

$$TiO_2 + 6F^- + 4H^+ \rightarrow [TiF_6]^{2-} + 2H_2O \tag{4}$$

Based on the traditional field-assisted dissolution mechanism, the inner diameter of nanotube mainly depends on the exposure to electrolyte due to the presence of chemical dissolution.[32,33] Long time exposition to fluorine containing electrolyte results in continuous thinning of the tube walls. TiO_2 nanotubes on the top are easier to be exposed to the electrolyte for longer time than those at the bottom. Thus, nanotube wall near the top ought to be thinner than that near the bottom and TiO_2 nanotubes formed in NH_4F-containing electrolyte show a V-shaped structure. In other words, A-shape profile (Fig. 1b3–

d3) could not be formed by chemical dissolution of formed TiO_2. Hence, the A-shaped sidewall thickness profile of nanotubes formed in HBF_4-containing electrolyte could hardly be explained by traditional field-assisted dissolution mechanism.

Moreover, the chemical dissolution of nanotube walls is continuous. If the multilayer TiO_2 nanotubes are formed by field-assisted dissolution process, what is the reason for periodically dissolution of oxide between layers? Taveira *et al.*[25] obtained two-layer TiO_2 nanotubes on titanium under galvanostatic condition. They suggested that big voltage oscillations triggered a detachment of the upper layer from the lower one.[25] The reason for voltage oscillations is still unclear. But there was no distinct voltage oscillation during the anodization in HBF_4-containing electrolyte, therefore, the multilayer TiO_2 nanotubes were not formed by voltage oscillations.

As indicated above, the formation of nanotubes with A-shape profile in HBF_4-containing electrolyte cannot be attributed to field-assisted dissolution effect of F^-. Although the BF_4^- could decompose to BF_3 and F^- under high electric field (eqn (5)),[39] field-assisted dissolution effect is not crucial for the formation of multilayer TiO_2 nanotubes.

$$BF_4^- \rightarrow BF_3 + F^- \tag{5}$$

According to previous works, the formation of TiO_2 nanotube is attributed to the flow of formed oxide around oxygen bubbles. Total anodizing current is composed of ionic current and electronic current.[16,19,40–43] Ionic current is used to form oxide while electronic current is used to form oxygen bubbles.[16,19,40–43] Nanotubes are formed by the combined effect of oxide formation and oxygen bubble expansion.[16,19,40–43]

Fig. 3 shows the measured voltage–time curves in HBF_4-containing electrolyte and NH_4F-containing electrolyte at same anodizing current. However, the equilibrium voltage in HBF_4-containing electrolyte is approximately twice as high as that in NH_4F-containing electrolyte. Voltage oscillations during anodization in HBF_4-containing electrolyte are more obvious than that in NH_4F-containing electrolyte.

Fig. 4 depicts the growth phases of multilayer TiO_2 nanotubes schematically. At the beginning of stage I, oxide is formed

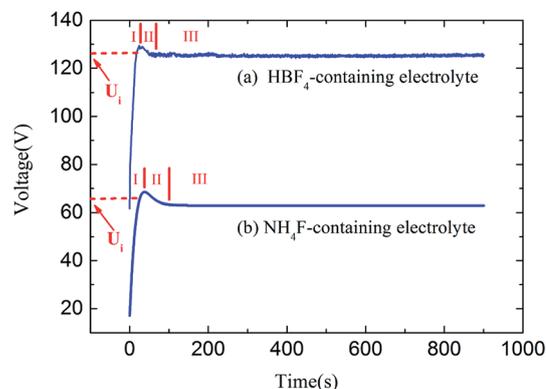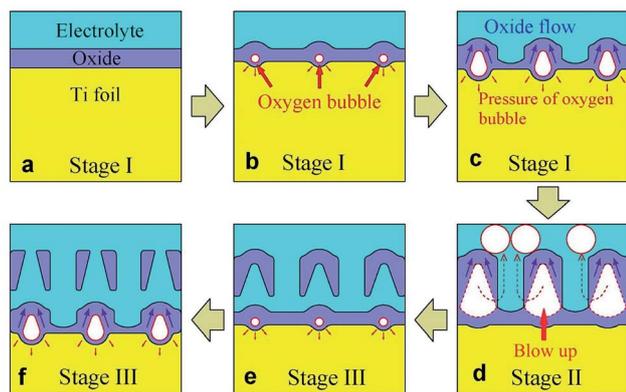**Fig. 3** Voltage–time curves during Ti anodizations in (a) HBF_4-containing electrolyte and (b) NH_4F-containing electrolyte.

Fig. 4 Schematic diagrams showing three growth stages of multilayer anodic TiO$_2$ nanotubes formed in HBF$_4$-containing electrolyte.

at electrolyte/metal interface (Fig. 4a). Anions migrate from electrolyte/oxide interface to oxide/metal interface, while cations migrate in the opposite direction. The total anodic current is ionic current which is induced by the migration of cations and anions in stage I. Owing to the oxidation reaction of cations and anions (eqn (1)–(3)), oxide grows at both interfaces (Fig. 4a). Therefore, all the anodic current is used to form oxide layer. Thickness of the oxide layer increases quickly and is directly proportional to the anodizing time. Resistance of the oxide layer is also directly proportional to the anodizing time. Therefore, the anodic potential is also directly proportional to the anodizing time at the beginning of stage I (Fig. 3). It is well known that the oxide layer could not be thickened infinitely. When the thickness of oxide layer reaches a critical value, the increase rate of the anodic potential will start to decline.

Since the thickness of oxide layer no longer increases, ionic current density should decrease. However, total anodic current density is constant. Where is the reduced portion of ionic current density? Cao et al.[44] and Anitha et al.[45] considered the dissolution current density as the reduced part of ionic current density. However, Prakasam et al.[46] indicated that chemical dissolution of oxide at the pore bottom does not contribute to the anodic current density. Thompson et al.[47] also thought that the dissolution reaction of the oxide is chemical in nature and does not contribute to anodic current. In fact, electronic current arises from dielectric breakdown of oxide. Electronic current density (j_e) increases exponentially with the increase of oxide thickness (eqn (6)).[18]

$$j_e = j_{e0} \times \exp(\theta d) \tag{6}$$

where, j_e is electronic current density, j_{e0} is initial electronic current density, θ is the impact ionization coefficient and d is oxide thickness.

Electronic current gives rise to oxygen bubbles in oxide (eqn (7) and Fig. 4b).

$$2O^{2-} = O_2\uparrow + 4e^- \tag{7}$$

Because of the pressure from electrolyte and formed oxide, oxygen bubbles can not escape from barrier layer into electrolyte immediately after they are formed (Fig. 4b).

As the electronic current increases with the oxide thickness, oxygen bubbles grow bigger and bigger in barrier layer (Fig. 4c). Newly formed oxide would flow upwards around oxygen bubbles.[19,40–43,45,48] The flow is suggested to be driven by the stresses caused by film growth and electric field.[16] In other words, the stresses are attributed to the electrostriction and volume change associated with oxidation of titanium.[16] Finally, the pressure in oxygen bubbles becomes bigger than the pressure of electrolyte and the formed oxide. Thus, oxygen bubbles start to escape (Fig. 4d).

It should be noted that the escape ways of oxygen bubbles in two electrolytes are different. In NH$_4$F-containing electrolyte, oxygen bubbles penetrate barrier layer and move upwards in nanotubes (Fig. 5a). However, in HBF$_4$-containing electrolyte, oxygen bubbles break TiO$_2$ nanotube sidewalls and move upwards in gaps between nanotubes (Fig. 5b). Difference between the two escape ways of oxygen bubbles could be attributed to the difference between magnitudes of ionic current and electronic current in two electrolytes. It is well known that at the inflection point (U_i) in stage I (Fig. 3a and b), thickness of barrier layer would reach a critical value (d_c).[18] Thickness of barrier layer would roughly keep constant during later anodization. Total anodizing current densities in two electrolytes are the same. Resistances of barrier layer in two electrolytes are proportional to thickness of barrier layer (d). The increase of potential in stage I is ascribed to the growth of barrier layer thickness under galvanostatic condition. Therefore, d_c is linearly proportional to the anodic potential at the inflection point (U_i). U_i in HBF$_4$-containing electrolyte (126.56 V) is higher than that in NH$_4$F-containing electrolyte (66.00 V). The value of d_c in HBF$_4$-containing electrolyte is nearly twice as big as that in NH$_4$F-containing electrolyte. After the inflection point, electronic current density exponentially increases (eqn (6)).[16,18,19] In HBF$_4$-containing electrolyte, thicker barrier layer presses oxygen bubbles against Ti substrates and nanotube walls. The growing oxygen bubbles are flattened by this pressure. As a consequence, the pressure in oxygen bubbles leads to thinner nanotube walls (Fig. 4c). Thus, oxygen bubbles will blow up from nanotube walls in HBF$_4$-containing electrolyte (Fig. 5b). Blowing up effect should account for the extremely thin nanotube walls at the bottom of nanotubes (Fig. 1b2 and c2). However, because barrier layer in NH$_4$F-containing electrolyte is

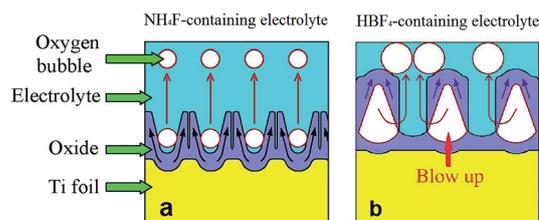Fig. 5 Schematic diagrams showing the escape ways of oxygen bubbles in (a) NH$_4$F-containing electrolyte and (b) HBF$_4$-containing electrolyte.

about half of that in HBF_4-containing electrolyte, oxygen bubbles in NH_4F-containing electrolyte would blow up from their upper oxide layer (Fig. 5a).

We name the pressure in oxygen bubble when it escapes from oxide as escaping pressure. Because of the thicker barrier layer, escaping pressure in oxygen bubble in HBF_4-containing electrolyte is higher than that in NH_4F-containing electrolyte. Therefore, diameters of escaped oxygen bubbles in HBF_4-containing electrolyte are bigger than in that NH_4F-containing electrolyte. In HBF_4-containing electrolyte, the inner diameters at the bottom of nanotubes in first and middle layer are close to the outer diameters (90 nm in Fig. 1b2, 72 nm in Fig. 1c2). However, the inner bottom diameter of TiO_2 nanotubes formed in NH_4F-containing electrolyte is 45 nm (inset of Fig. 2b). Yu et al.[43] suggested that the inner bottom diameter of TiO_2 nanotubes is close related to the diameter of escaped oxygen bubbles. Thus, the escaped oxygen bubbles in HBF_4-containing electrolyte are bigger than those in NH_4F-containing electrolyte. In the following anodization process, escape of bigger oxygen bubbles results in much larger potential oscillations in HBF_4-containing electrolyte than that in NH_4F-containing electrolyte.

After oxygen bubbles escape from barrier layer, electrolyte enters the pores left by oxygen bubbles, which leads to the decrease of potential (stage II, Fig. 4d). Taveira et al.[25] suggested that an easy access of electrolyte was formed on the broken area of nanotubes, which led to the decrease of potential. When all of the TiO_2 nanotube walls are broken by oxygen bubbles, anodizing potential is lowest, and anodization reaches stage III. New oxygen bubbles will be formed by electronic current during subsequent anodization (Fig. 4e).

In stage III, the anodic potential and thickness of barrier layer both kept roughly constant. Oxygen bubbles were formed continuously and then blow up in barrier layer. Oxide flows upwards around oxygen bubbles, and therefore nanotubes are formed. In HBF_4-containing electrolyte, oxygen bubbles grow and broaden the bottom of anodic TiO_2 nanotubes. Then oxygen bubbles blow up through the sidewalls of nanotubes (Fig. 4d and 5b). Accordingly, the A-shaped sidewall thickness profiles of TiO_2 nanotubes are formed. And at the same time, the extremely thin sidewall at the nanotube bottoms would be damaged by the released oxygen bubbles, thus resulting in an individual layer of TiO_2 nanotubes (Fig. 4e). In NH_4F-containing electrolyte, oxygen bubbles move upwards in nanotubes. Due to the lower pressure of electrolyte on the top of nanotubes, oxygen bubbles expand the inner diameters at the top of nanotubes. Owing to the movement and expansion of oxygen bubbles, V-shaped TiO_2 nanotubes are finally formed in NH_4F-containing electrolyte (Fig. 5a). In HBF_4-containing electrolyte, oxygen bubbles moved upwards in gaps between TiO_2 nanotubes and separated neighbouring TiO_2 nanotubes. Thus TiO_2 nanotubes were spaced in top image in HBF_4-containing electrolyte (Fig. 1b1). However, oxygen bubbles moved upwards inside TiO_2 nanotubes, and as a result, TiO_2 nanotubes were not spaced in top image in NH_4F-containing electrolyte (Fig. 2a).

It should be noted that the oxide layer on the top of anodic TiO_2 nanotubes will be dissolved by HBF_4-containing electrolyte (Fig. 4f). Therefore, we obtained the final anodic TiO_2 nanotubes with through holes on the top (Fig. 1b).

Due to the damage of nanotube walls by oxygen bubbles, the whole TiO_2 nanotube layer is divided to nanotube multilayers (Fig. 4f). Nevertheless, oxygen bubbles do not blow up exactly at the same time because the surface of Ti substrate is of great unevenness. As a consequence, anodic potential–time curve was not regularly pulsating during anodizing in HBF_4-containing electrolyte. The oxygen bubbles' blowing up effect is the reason for the division of TiO_2 nanotube layer and the oscillation of anodizing potential.

In summary, electrochemical reactions of anodizations in HBF_4-containing electrolyte and NH_4F-containing electrolyte are similar. Different magnitudes of ionic current and electronic current in two electrolytes result in different volumes of escaped oxygen bubbles and different escape ways of oxygen bubbles, thus different architectures of TiO_2 nanotubes are formed. Due to the damage of nanotube walls by oxygen bubbles, the TiO_2 nanotube layer is divided to multilayers in HBF_4-containing electrolyte.

Conclusions

When the anodization of titanium was performed in HBF_4-containing electrolyte, multilayer anodic TiO_2 nanotubes were obtained. Nanotubes in the middle layers show a unique A-shaped sidewall thickness profile. Formation mechanism of the multilayer anodic TiO_2 nanotubes and A-shaped sidewall thickness profile could not be explained by traditional field-assisted dissolution mechanism. And then a possible formation mechanism of the multilayer anodic TiO_2 nanotubes is proposed. Migration of ions forms ionic current and produces oxide. Oxygen bubbles, which arise from the electronic current, act as moulds during oxide growth. Oxide flows around oxygen bubbles and forms nanotubes. Unlike the formation of nanotubes in NH_4F-containing electrolyte where oxygen bubbles escape from barrier layer and move upwards in nanotubes, in HBF_4-containing electrolyte, oxygen bubbles break nanotube walls and move upwards in gaps between nanotubes. Therefore, the unique escape way of oxygen bubbles formed the A-shaped sidewall thickness profile and homogeneous nanotube multilayers in the HBF_4-containing electrolyte.

Acknowledgements

References

1 H. Mokarami Ghartavol, M. Mohammadi, A. Afshar, F. C.-N. Hong and Y.-R. Jeng, RSC Adv., 2016, 6, 101737.
2 J. M. Hernández-López, A. Conde, J. J. de Damborenea and M. A. Arenas, RSC Adv., 2014, 4, 62576.

3 S. Chen, M. Liao, P. Yang, S. Yan, R. Jin and X. Zhu, *RSC Adv.*, 2016, **6**, 84309.

4 L. X. Zheng, Y. C. Dong, H. D. Bian, C. Lee, J. Lu and Y. Y. Li, *Electrochim. Acta*, 2016, **203**, 257.

5 D. Yu, X. Zhu, Z. Xu, X. Zhong, Q. Gui, Y. Song, S. Zhang, X. Chen and D. Li, *ACS Appl. Mater. Interfaces*, 2014, **6**, 8001.

6 V. Zwilling, M. Aucouturier and E. Darque-Ceretti, *Electrochim. Acta*, 1999, **45**, 921.

7 J. M. Macak, K. Sirotna and P. Schmuki, *Electrochim. Acta*, 2005, **50**, 3679.

8 J. M. Macák, H. Tsuchiya and P. Schmuki, *Angew. Chem., Int. Ed.*, 2005, **44**, 2100.

9 L. V. Taveira, J. M. Macák, H. Tsuchiya, L. F. P. Dick and P. Schmuki, *J. Electrochem. Soc.*, 2005, **152**, B405.

10 D. Regonini, C. R. Bowen, A. Jaroenworaluck and R. Stevens, *Mater. Sci. Eng., R*, 2013, **74**, 377.

11 C. Richter, Z. Wu, E. Panaitescu, R. Willey and L. Menon, *Adv. Mater.*, 2007, **19**, 946.

12 N. F. Fahim, T. Sekino, M. F. Morks and T. Kusunose, *J. Nanosci. Nanotechnol.*, 2009, **9**, 1803.

13 C. Chang, X. Huang, Y. Liu, L. Bai, X. Yang, R. Hang, B. Tang and P. K. Chu, *Electrochim. Acta*, 2015, **173**, 345.

14 F. Hu, X. Lin, S. L. Zhu, X. J. Yang and Z. D. Cui, *Appl. Surf. Sci.*, 2012, **258**, 3260.

15 Ö. Ö. Çapraz, P. Shrotriya, P. Skeldon, G. E. Thompson and K. R. Hebert, *Electrochim. Acta*, 2015, **167**, 404.

16 R. Yang, L. Jiang, X. Zhu, Y. Song, D. Yu and A. Han, *RSC Adv.*, 2012, **2**, 12474.

17 Y. Zhang, D. Yu, M. Gao, D. Li, Y. Song, R. Jin, W. Ma and X. Zhu, *Electrochim. Acta*, 2015, **160**, 33.

18 B. Chong, D. Yu, R. Jin, Y. Wang, D. Li, Y. Song, M. Gao and X. Zhu, *Nanotechnology*, 2015, **26**, 145603.

19 Y. Zhang, H. Fan, X. Ding, Q. Yan, L. Wang and W. Ma, *Electrochim. Acta*, 2015, **176**, 1083.

20 J. Xing, H. Li, Z. Xia, J. Chen, Y. Zhang and L. Zhong, *Electrochim. Acta*, 2014, **134**, 242.

21 K. Lee, A. Mazare and P. Schmuki, *Chem. Rev.*, 2014, **114**, 9385.

22 P. Roy, S. Berger and P. Schmuki, *Angew. Chem., Int. Ed.*, 2011, **50**, 2904.

23 A. Baron-Wiecheć, M. G. Burke, T. Hashimoto, H. Liu, P. Skeldon, G. E. Thompson, H. Habazaki, J. J. Ganem and I. C. Vickridge, *Electrochim. Acta*, 2013, **113**, 302.

24 J. M. Montero-Moreno, M. Sarret and C. Müller, *Microporous Mesoporous Mater.*, 2010, **136**, 68.

25 L. V. Taveira, J. M. Macak, K. Sirotna, L. F. P. Dick and P. Schmuki, *J. Electrochem. Soc.*, 2006, **153**, B137.

26 Y. Zhang, W. Cheng, F. Du, S. Zhang, W. Ma, D. Li, Y. Song and X. Zhu, *Electrochim. Acta*, 2015, **180**, 147.

27 S. P. Albu, D. Kim and P. Schmuki, *Angew. Chem., Int. Ed.*, 2008, **120**, 1942.

28 X. Zhou, N. T. Nguyen, S. Özkan and P. Schmuki, *Electrochem. Commun.*, 2014, **46**, 157.

29 V. C. Anitha, A. N. Banerjee, S. W. Joo and B. K. Min, *Mater. Sci. Eng., B*, 2015, **195**, 1.

30 X. Wang, L. Sun, S. Zhang and D. Zhao, *Electrochim. Acta*, 2013, **107**, 200.

31 D. Kowalski, D. Kim and P. Schmuki, *Nano Today*, 2013, **8**, 235.

32 S. P. Albu, A. Ghicov, S. Aldabergenova, P. Drechsel, D. LeClere, G. E. Thompson, J. M. Macak and P. Schmuki, *Adv. Mater.*, 2008, **20**, 4135.

33 K. Yasuda and P. Schmuki, *Electrochim. Acta*, 2007, **52**, 4053.

34 Z. Su and W. Zhou, *Adv. Mater.*, 2008, **20**, 3663.

35 M. Paulose, H. E. Prakasam, O. K. Varghese, L. Peng, K. C. Popat, G. K. Mor, T. A. Desai and C. A. Grimes, *J. Phys. Chem. C*, 2007, **111**, 14992.

36 W. Krengvirat, S. Sreekantan, A. F. M. Noor, G. Kawamura, H. Muto and A. Matsuda, *Electrochim. Acta*, 2013, **89**, 585.

37 J. M. Macak, H. Hildebrand, U. Marten-Jahns and P. Schmuki, *J. Electroanal. Chem.*, 2008, **621**, 254.

38 G. K. Mor, O. K. Varghese, M. Paulose, K. Shankar and C. A. Grimes, *Sol. Energy Mater. Sol. Cells*, 2006, **90**, 2011.

39 L. Xiao and K. E. Johnson, *J. Electrochem. Soc.*, 2003, **150**, E307.

40 X. Zhu, Y. Song, D. Yu, C. Zhang and W. Yao, *Electrochem. Commun.*, 2013, **29**, 71.

41 Y. Li, Z. Y. Ling, X. Hu, Y. Liu and Y. Chang, *RSC Adv.*, 2012, **2**, 5164.

42 X. M. Zhong, D. L. Yu, S. Y. Zhang, X. Chen, Y. Song, D. D. Li and X. F. Zhu, *J. Electrochem. Soc.*, 2013, **160**, E125.

43 D. Yu, S. Zhang, X. Zhu, H. Ma, H. Han and Y. Song, *J. Solid State Electrochem.*, 2014, **18**, 2609.

44 C. Cao, J. Li, X. Wang, X. Song and Z. Sun, *J. Mater. Res.*, 2011, **26**, 437.

45 V. Anitha, A. Banerjee, S. W. Joo and B. K. Min, *Mater. Sci. Eng., B*, 2015, **195**, 1.

46 H. E. Prakasam, K. Shankar, M. Paulose, O. K. Varghese and C. A. Grimes, *J. Phys. Chem. C*, 2007, **111**, 7235.

47 J. Oh and C. V. Thompson, *Electrochim. Acta*, 2011, **56**, 4044.

48 S. Y. Zhang, D. L. Yu, D. D. Li, Y. Song, J. F. Che, S. Y. You and X. F. Zhu, *J. Electrochem. Soc.*, 2014, **161**, E135.